ACS OMEGA

http://pubs.acs.org/journal/acsodf

Article

Novel Bending Sensor Based on a Solution-Processed Cu_2O Film with High Resolution Covering a Wide Curvature Range

Ryosuke Nitta, Ryo Taguchi, Yuta Kubota, Tetsuo Kishi, Atsushi Shishido, and Nobuhiro Matsushita*

Cite This: *ACS Omega* 2021, 6, 32647−32654

Read Online

ACCESS | Metrics & More | Article Recommendations

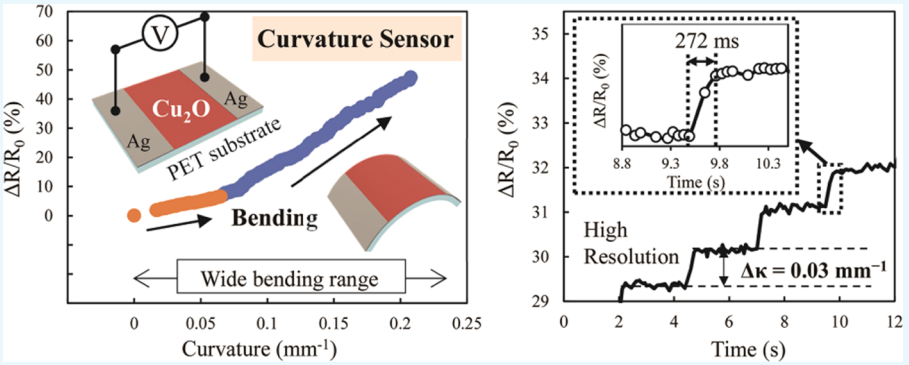

ABSTRACT: A Cu_2O film is prepared on a flexible polyethylene terephthalate substrate for a bending sensor using the spin−spray method, a facile and low-environmental-load solution process. The Cu_2O bending sensor shows high sensitivity and high resolution not only over a wide range of curvatures ($0 < \kappa < 0.21$ mm^{-1}) but also for very small curvature changes ($\Delta\kappa = \sim 0.03$ mm^{-1}). The bending response of the sensor exhibited a curvature change of high linearity with a good gauge factor (18.2) owing to the grain-boundary resistance and piezoresistive effects of the fabricated Cu_2O film. In addition, the sensor possesses good repeatability, stability, and long-term (>30 days) and mechanical fatigue durability (1000 bending−release cycles). The sensor is capable of detailed monitoring of large- and small-scale human motions, such as finger bending, wrist bending, nodding, mouth opening/closing, and swallowing. In addition, excellent stability and repeatability of the monitoring performance is observed over a wide range of motion angles and speeds. All of these results demonstrate the potential of the flexible bending sensor based on the Cu_2O film as a candidate for healthcare monitoring and wearable electronics.

1. INTRODUCTION

Recently, flexible bending sensors have attracted considerable attention owing to their various applications in human motion monitoring, healthcare monitoring, and soft robotics.[1−3] A wide variety of bending sensors based on capacitors, transistors, piezoelectric nanogenerators, and piezoresistive materials have been developed.[4−6] Among these sensors, piezoresistive sensors are extremely attractive because of their high sensitivity, fast response time, feasible fabrication, and easy signal collection.[7−9] Typically, this type of bending sensor is composed of a flexible polymer substrate and piezoresistive sensing materials. Various types of piezoresistive materials, including metal materials, conductive polymers, and metal oxide semiconductors (SMOs), have been used to fabricate bending sensors.[1,10,11] Generally, metal materials and conductive polymers are expensive, have low long-term stability, and require complex and high-cost fabrication methods. On the other hand, the advantages of SMOs, including their nontoxicity, low cost, and long-term durability, are of great significance in the development of bending sensors for human motion detection.[12,13] However, it is difficult to fabricate SMO films on flexible polymer substrates with low heat and chemical durability due to their high fabrication temperature and complex processes. Therefore, there were few reports on flexible bending sensors based on SMOs.

Cuprous oxide (Cu_2O) is a p-type SMO with a direct band gap of ∼2.17 eV and a cubic cupric structure.[14] Cu_2O films have generated significant interest for a wide range of applications including catalysts, gas sensors, biosensors, and solar cells owing to their natural abundance, nontoxicity, and chemical stability.[15−19] In addition, these characteristics indicate that Cu_2O films are promising sensing materials for

Received: August 9, 2021
Accepted: October 11, 2021
Published: November 8, 2021

wearable sensors. However, there have been no reports on bending sensors for wearable device applications based on Cu_2O films. Over the past decades, various physical and chemical methods, such as rf sputtering, chemical vapor deposition, chemical bath deposition, sol−gel processing, and electrochemical deposition, have been proposed to fabricate Cu_2O films.[20−25] These conventional methods limit the substrate choice because they require high fabrication temperatures, a chemically resistant substrate, and/or a conductive substrate. Therefore, it is difficult to manufacture a "flexible" Cu_2O film for bending sensor application using flexible polymer substrates such as polyimide (PI) or poly(ethylene terephthalate) (PET) with low heat and chemical durability.

To overcome the issues presented by conventional fabrication methods and to obtain good adhesion between the sensing material and the substrate, the spin−spray method has been applied to fabricate flexible bending sensors based on Cu_2O films, as shown in Figure 1a. We previously fabricated

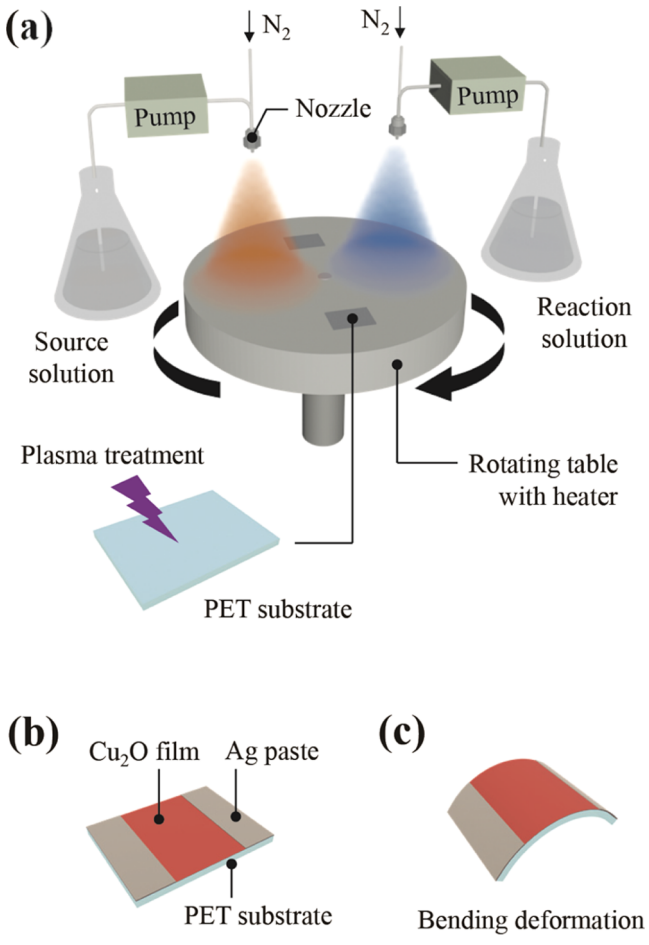

Figure 1. Schematic illustration of (a) spin−spray method, (b) fabricated Cu_2O bending sensor, and (c) bending sensor subjected to bending deformation.

phase-pure Cu_2O films on glass substrates at 70 °C with a high deposition rate of ∼0.3 μm/min using this method.[26] The detailed fabrication mechanism of the spin−spray method is discussed in our previous report. In addition, our groups have reported the fabrication of metal oxides such as Fe_3O_4, ZnO, and SnO_2 on substrates at temperatures below 100 °C using this method.[27−29] Importantly, this method does not adversely affect the substrate because of the low fabrication temperature and a high deposition rate, which allows a short deposition time.

In this study, a phase-pure Cu_2O film was fabricated on a flexible PET substrate with good adhesion using the spin−spray method. The fabricated sample was employed as a flexible bending sensor, and its bending performance was evaluated by measuring the electrical resistance between the electrodes under various curvatures. The Cu_2O bending sensor showed high sensitivity and high resolution not only over a wide range of curvatures ($0 < \kappa < 0.21$ mm^{-1}) but also for very small curvature changes ($\Delta\kappa = \sim 0.03$ mm^{-1}). In addition, the sensor possessed high linearity with a high GF (18.2) and long-term (>30 days) and mechanical fatigue durability (1000 bending−release cycles). These sensor properties would be useful in monitoring both large- and small-scale human motions such as finger bending, wrist bending, nodding, and swallowing.

2. RESULTS AND DISCUSSION

2.1. Sample Characterization. The spin−spray method enabled the one-step fabrication of a Cu_2O film at a low temperature of 70 °C with a high deposition rate of >0.35 μm/min. Because this method results in low heat damage of the substrate during fabrication, the fabrication could be achieved even on the PET substrate with low thermal durability. Figure 2a shows the uniformly deposited, orange sample on the substrate. The film exhibited strong adhesion to the substrate without peeling off, even after ultrasonication at 45 kHz of 200 W in deionized water for 10 min.

Our previous study suggested that Cu^+ ions in the source solution reacted with OH^- ions in the reaction solution to form Cu_2O on the substrate, as shown in eq 1.[26]

$$2Cu^+ + 2OH^- \rightarrow 2CuOH \rightarrow Cu_2O + H_2O \quad (1)$$

It is important for the fabrication of metal oxide films by the spin−spray method to increase the hydrophilicity of the substrate surface by the plasma treatment before the film fabrication. There were a large number of polar functional groups such as carbonyl, hydroxyl, and aldehyde/ketone (−COOH, −OH, and −CO), on the surface of the PET substrate due to the hydrophilicity caused by plasma treatment.[30] The formed crystal nuclei of Cu_2O due to heterogeneous nucleation were chemically bonded to the functional groups on the substrate surface and grew to form a Cu_2O film, as indicated in eq 2. Therefore, the film fabricated by the spin−spray method exhibited strong adhesion to the substrate. Figure 2b shows the surface and cross-sectional SEM images of the sample. The 3.56 μm thick film was uniform with a relatively flat surface and composed of submicron-sized grains, as shown in Figure 2b. The spin−spray method enabled the fabrication of a Cu_2O film with larger particle size at a higher deposition rate than the Cu_2O films fabricated by other methods. As shown in our previous study, each of NaOH and NH_3 aq. components in the reaction solution played an important role in the fabrication of the Cu_2O film.[26] NaOH provided OH^- ions to the reaction field on the rotating table and promoted the chemical reaction of eq 2. The spin−spray method achieved a high deposition rate of >0.35 μm/min using a reaction solution containing a high concentration of NaOH (0.4 M). However, NH_3 dissolved the surface part of the growing Cu_2O film, as shown in eq 2, and the dissolution

https://doi.org/10.1021/acsomega.1c04279
ACS Omega 2021, 6, 32647−32654

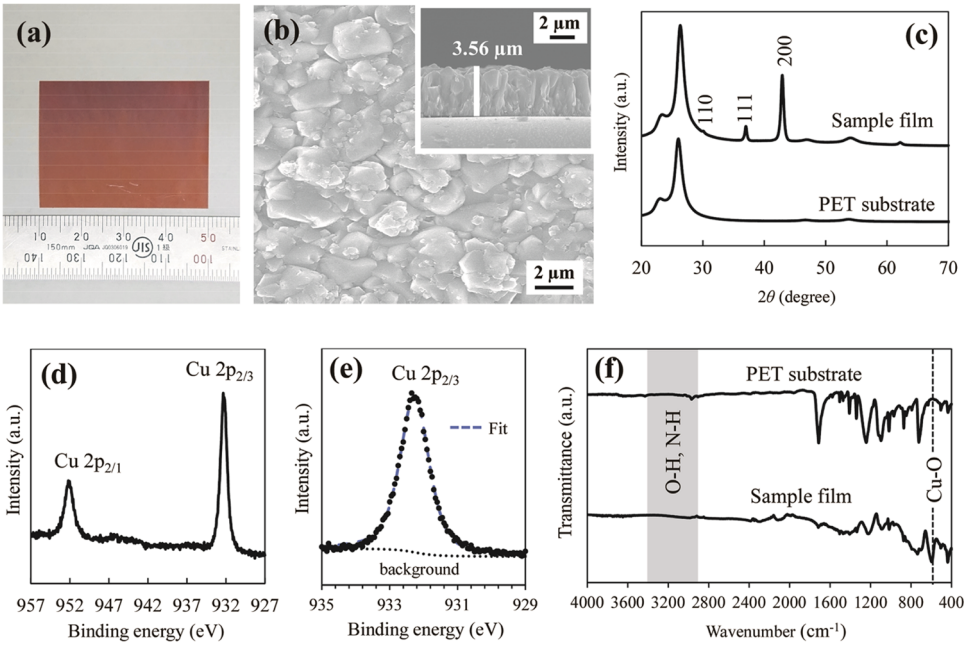

Figure 2. (a) Photograph of the fabricated Cu_2O film, (b) surface and cross-sectional field-emission scanning electron microscopy (FESEM) image of the sample film, (c) X-ray diffraction (XRD) patterns of the sample film and the PET substrate, (d) X-ray photoelectron spectroscopy (XPS) Cu 2p spectra of the sample film, (e) XPS curve fitting of the Cu $2p_{2/3}$ peak, and (f) attenuated total reflection Fourier transform infrared (ATR-FTIR) spectra of the sample film.

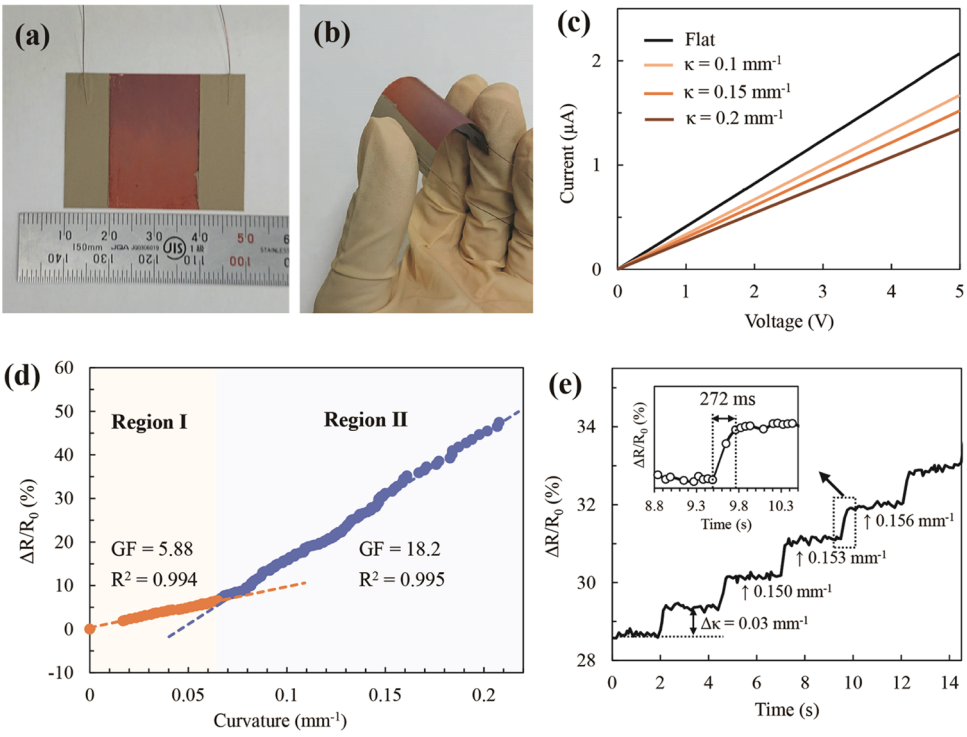

Figure 3. (a) Photographs of the fabricated Cu_2O bending sensor; (b) photographs of the bending sensor under a bent condition; (c) $I-V$ curves of the bending sensor in bending with curvatures of 0, 0.10, 0.15, and 0.20 mm^{-1}; (d) resistance variation of the bending sensor under a wide range of bending with curvatures between 0 and 0.21 mm^{-1}; and (e) resistance variation of the bending sensor held at curvatures of 0.145, 0.147, 0.150, 0.153, and 0.156 mm^{-1} for 5 s.

and reprecipitation occurred simultaneously on the film surface for the fabrication using the reaction solution containing a high concentration of NH_3 (1.2 M).

$$Cu_2O + 4NH_3 + H_2O \rightarrow CU(NH_3)_2^{+} + 2OH^{-} \quad (2)$$

The Cu_2O film fabricated by the spin−spray method had large grain sizes due to Ostwald ripening, where small crystals were dissolved and then reprecipitated on large crystals.

The structural properties of the sample on the PET substrate were characterized by XRD, and the obtained patterns are

https://doi.org/10.1021/acsomega.1c04279
ACS Omega 2021, 6, 32647−32654

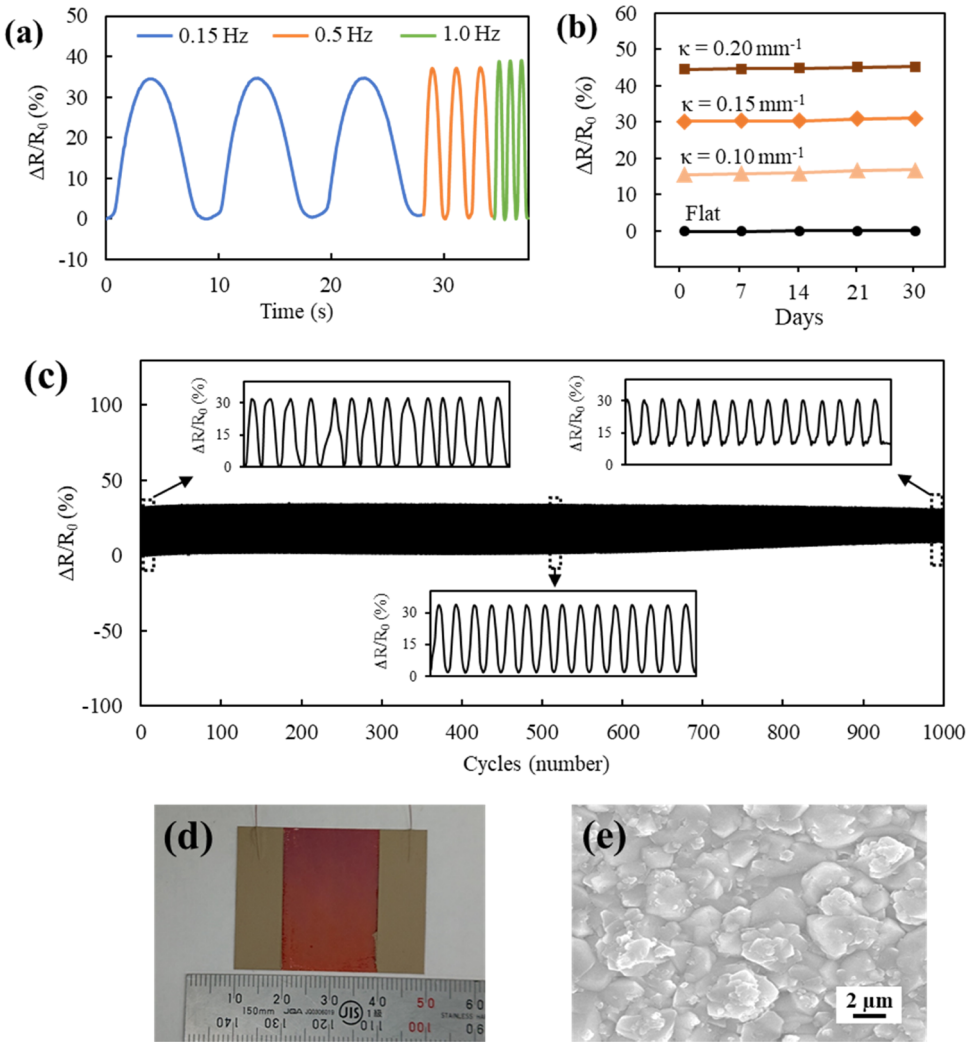

Figure 4. Resistance variation of the bending sensor (a) under bending−release cycle between curvatures of 0 and ∼0.16 mm^{-1} at a frequency of 0.15, 0.5, and 1.0 Hz, (b) at curvatures of 0, 0.10, 0.15, and 0.20 mm−1 for 30 days at intervals of several days, and (c) for 1000 bending−release cycles between curvatures of 0 and ∼0.16 mm^{-1} at a frequency of 1.0 Hz. (d) Photograph and (e) surface FESEM image of the Cu_2O bending sensor after 1000 bending−release cycles.

shown in Figure 2c. The XRD peaks corresponded to the cubic phase of Cu_2O in good accordance with the ICCD data (No. 77-0199) in addition to PET peaks without the presence of impurity peaks from $Cu(OH)_2$ or CuO. The presence of impurities in the sample was further analyzed using XPS and ATR-FTIR. Figure 2f presents the XPS spectra of the Cu2p region for the sample. The peaks at 932.4 and 952.2 eV correspond to Cu $2p_{3/2}$ and Cu $2p_{1/2}$, respectively, indicating the presence of Cu^+.[31] As shown in Figure 2e, the Cu $2p_{3/2}$ peak could be fitted to a single peak with a binding energy of 932.4 eV. These XPS results indicate the pure phase formation of Cu_2O without impurities such as metal Cu, CuO, and $Cu(OH)_2$. Figure 2d presents the ATR-FTIR spectra of the sample. The band at approximately 600 cm^{-1} is attributed to the vibrational mode of Cu−O in Cu_2O.[32] No band was present between 3000 and 3500 cm^{-1}, which corresponds to the region of O−H and N−H stretching, and no ascorbic acid-related bands were detected.[33,34] The ATR-FTIR results indicate that the sample film did not contain any impurities, such as water, amines, or ascorbic acid. The fabrication of a phase-pure Cu_2O film by the spin−spray method can be explained as follows. Copper ions in the source solution were fully reduced by ascorbic acid, and the fresh source solution was supplied continuously onto the substrate fixed on the rotating table. The use of a solution containing only Cu^+ ions and free from Cu^{2+} ions was one key factor in fabricating a phase-pure Cu_2O film without impurities. Another key factor was the removal of unreacted solution from the substrate surface during film deposition via a centrifuge.

The previous study provides more details on the fabrication mechanism of a Cu_2O film via the spin−spray method.[26]

2.2. Bending Sensor Performance of a Cu_2O Film.

Figure 3a shows photographs of the bending sensor based on the Cu_2O film fabricated by the spin−spray method. The sensor was sufficiently flexible to be used in bent conditions, as shown in Figure 3b. The curvature (κ) was the most appropriate criterion to evaluate the bending characteristics, and thus, in the present study, the bending performance was evaluated by measuring the electrical resistance between the electrodes under various curvatures.[35] Figure 3c shows the $I-V$ curves of the sensor in bending with various curvatures such as 0, 0.10, 0.15, and 0.20 mm^{-1}. An excellent linear relationship between the voltages and currents is observed in all of the $I-V$ curves, indicating the Ohmic behavior and constant resistance

https://doi.org/10.1021/acsomega.1c04279
ACS Omega 2021, 6, 32647−32654

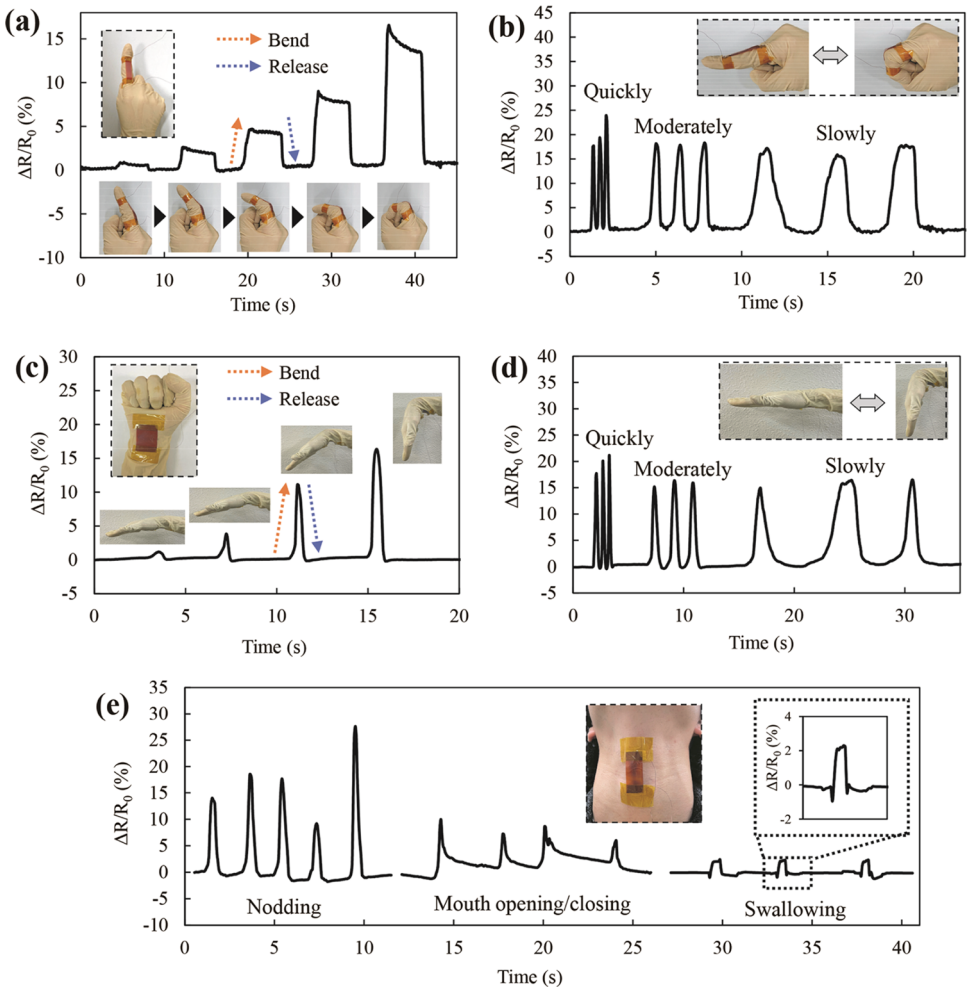

Figure 5. Real-time monitoring of human motions by the bending sensor. Sensing curves of the bending sensor attached on an index finger under different (a) motion angles and (b) motion speeds; the inset presents photographs of the finger bending to the corresponding positions. Sensing curves of the bending sensor attached on a wrist under different (c) motion angles and (d) motion speeds; the inset presents photographs of the wrist bending to the corresponding positions. (e) Nodding, mouth opening/closing, and swallowing sensing by attaching the bending sensor to the throat; the inset presents photographs of the bending sensor attached to the throat.

of the sensor in the static state. The slope of the $I-V$ curves, which is negatively correlated to the resistance, decreased significantly as the curvature increased, demonstrating excellent electromechanical performance. To further evaluate the electrical bending sensing performance, the relative resistance variation ($\Delta R/R_0$, where ΔR is the relative change in resistance and R_0 is the resistance of the Cu_2O bending sensor under the flat state) were measured under various curvatures, as shown in Figure 3d. The sensor responded to a wide range of bending with curvatures between 0 and 0.21 mm^{-1}. We analyzed the result of Figure 3d by evaluating the sensor sensitivity using GF, which is defined as GF = $(\Delta R/R_0)/\varepsilon$, where ε is the surface bending strain. The value of ε can be calculated using the formula $\varepsilon = (d \times \kappa)/2$, where d is the thickness of the PET substrate and κ is the applied curvature.[36] In the present study, d is 0.125 mm. As shown in Figure 3d, the curve of the resistance variation in the perpendicular bending versus curvature can be divided into two linear parts, region I ($0 < \kappa < 0.05$ mm^{-1}) and region II ($0.05 < \kappa < 0.20$ mm^{-1}) with coefficients of determination of 0.994 and 0.995, respectively. As shown in Figure 3e, the GF values in the two regions were 5.88 and 18.2, respectively. The high linearity and good GF values in the two regions ensured that the sensor possesses excellent sensing properties.

In region I ($0 < \kappa < 0.05$ mm^{-1}), the linear response of the Cu_2O-based sensor is due to the piezoresistive effect in the Cu_2O film, which is a p-type semiconductor. In semiconductors, the changes in resistivity are related to the change in mobility induced by the lattice deformation.[37] In general, the resistivity of p-type semiconductors increases linearly with respect to the strain due to the increase of the hole population with decreased mobility by the deformation.[38] This characterization of the piezoresistive effect is consistent with the result in region I of Figure 3d, showing the sensing performance with high linearity. However, the bending sensing performance in region II ($0.05 < \kappa < 0.20$ mm^{-1}) is due not only to the piezoresistive effect but also to the "grain-boundary resistance effect". As shown in Figure 2b, there are many grain boundaries in the polycrystalline Cu_2O film composed of submicron-sized grains. The bending would lead to the expansion of the distance between the grains along the bending direction, resulting in the increase of grain-boundary resistance.[39] Because the distance between the grains expands in proportion to the applied strain (ε), the resistance variation in the bending changes linearly with the curvature (κ)

https://doi.org/10.1021/acsomega.1c04279
ACS Omega 2021, 6, 32647−32654

calculated from the formula $\kappa = (2/d) \times \varepsilon$.[40] The combined effect of this grain-boundary resistance and the piezoresistive effect led to the high linear response of the Cu_2O bending sensor shown in region II.

To evaluate the resolution of the Cu_2O bending sensor, the sensing response to minute changes in curvature was investigated. Figure 3e shows the resistance variation of the sensor held at various curvatures (0.145, 0.147, 0.150, 0.153, and 0.156 mm^{-1}) for 5 s. The sensor responded to very small curvature changes ($\Delta\kappa$ = ~0.03 mm^{-1}, i.e., $\Delta\varepsilon$ = ~ 1.88 × 10^{-3}), demonstrating the high-resolution performance. In addition, the sensor had a short response time (~272 ms) between curvatures of 0.153 and 0.156 mm^{-1}, as shown in Figure 3e.

The repeatability and long-term and mechanical fatigue durability are important characteristics of the sensor devices from the perspective of practical applications. Figure 4a shows the repeatability of the sensor investigated by exercising the bending−release cycle between curvatures of 0 and ~0.16 mm^{-1}. The result in Figure 4a demonstrates that the resistance variation of the sensor showed almost no frequency dependence in certain bending. Such a reliable response is essential for practical applications of bending sensors such as motion monitoring. The long-term stable nature of the sensor performance at various curvatures such as 0, 0.10, 0.15, and 0.20 mm^{-1} was examined for 30 days at intervals of several days, as shown in Figure 4b. The sensor was stored in a desiccator at 50−60% relative humidity and room temperature for the duration of the experiment. There was almost no change in the sensor resistance variation at any curvature over 30 days, indicating that the sensor possessed excellent long-term durability at room temperature. Figure 4c shows the fatigue testing of the sensor for 1000 bending−release cycles at 1.0 Hz between curvatures of 0 and ~0.16 mm^{-1}. There was almost no change in the resistance variation of the sensor up to 500 bending−release cycles, while the sensor resistance at the flat state increased slightly from 500 to 1000 bending−release cycles. The change in the resistance before and after the fatigue testing was approximately 10%. The sensor displayed good repeatability and reversibility even after approximately 1000 bending−release cycles, indicating the sufficient durability and stability of the sensor for practical applications. Figure 4d,e shows the photograph and the surface FESEM image of the Cu_2O bending sensor after 1000 bending−release cycles. As shown in Figure 4d, the Cu_2O film did not peel off from the PET substrate even after 1000 bending−release cycles, indicating the excellent adhesion between them. In addition, no microcracks were observed on the surface FESEM image of the sensor after the fatigue testing. The increase of about 10% in the sensor resistance after the fatigue testing was due to nanosized cracks in the films, which were too small to be observed by SEM. The thickness of the Cu_2O film was 3.56 μm, as shown in Figure 1b, which was small compared to the thickness of the PET substrate (0.125 mm). The applied strain of the film at the bending state can be approximated to the surface strain of the PET substrate. Therefore, the strain of the Cu_2O film when bending between the curvatures of 0 and 0.16 mm^{-1} was very small (0.01), indicating that the film was not deformed significantly.

2.3. Motion Sensor Applications of a Cu_2O Film. Given its excellent bending stability and sensitivity, the Cu_2O bending sensor can be used for wearable devices to detect human motions. The sensor, which is thin, flexible, and nontoxic, can be easily attached to the human body. In addition, this sensor can be easily cut with scissors to fit the size of the detection points on the human body. To demonstrate the feasibility of the Cu_2O bending sensor, a real-time detection example is shown in Figure 5. First, the sensor was cut and attached to the index finger to monitor the finger motion, as shown in Figure 5a. Figure 5a,b shows the real-time sensing curves toward the finger bending and stretching at various motion angles and speeds, respectively. In addition, the sensor was attached to the wrist to monitor specific wrist motions, as shown in Figure 5c,d. These results demonstrate the excellent stability and repeatability of the sensor over a wide range of motion angles and speeds. In addition, the sensor was cut and adhered directly to the throat to monitor neck, chin, and larynx motions, as shown in Figure 5e. Figure 5e shows the real-time response patterns for nodding, mouth opening/closing, and swallowing motions, which were caused by the neck, chin, and larynx movements, respectively. The sensor can monitor not only large-scale human activity such as nodding but also small-scale human motion such as mouth opening/closing and swallowing. All of these results demonstrate the potential application of the Cu_2O bending sensor for high-performance wearable electronic devices for healthcare monitoring.

3. CONCLUSIONS

The spin−spray method enabled the one-step fabrication of a Cu_2O film on a flexible PET substrate for application as a bending sensor. The 3.56 μm thick film was uniform with a relatively flat surface and composed of submicron-sized grains. The Cu_2O bending sensor possessed excellent stability and repeatability over a wide range of bending with curvatures between 0 and 0.21 mm^{-1}. The combination of this grain-boundary resistance effect and the piezoresistive effect led to a high linear response with a high GF value (18.2) in response to the curvature change. Moreover, the sensor demonstrated high sensitivity and a short response time of 272 ms with a high resolution for very small curvature changes ($\Delta\kappa$ = ~0.03 mm^{-1}). The sensor possessed good repeatability as well as long-term and mechanical fatigue durability over 30 days and 1000 bending−release cycles, respectively. All of these excellent sensing characteristics indicate the applicability of the sensor for detailed monitoring of large- and small-scale human motions, such as finger bending, wrist bending, nodding, mouth opening/closing, and swallowing. Excellent stability and repeatability of the monitoring response over a wide range of motion angles and speeds were demonstrated. Given its numerous advantages, the Cu_2O bending sensor has broad application prospects for future wearable electronics.

4. EXPERIMENTAL SECTION

4.1. Materials. PET substrates were purchased from Toray Industries, Inc., Japan. The Ag paste was purchased from KAKEN TECH Co., Ltd., Japan. Copper(II) sulfate pentahydrate ($CuSO_4 \cdot 5H_2O$, 99.0%), ascorbic acid ($C_6H_8O_6$, 99.0%), sodium hydroxide (NaOH, 99.0%), and ammonia (NH_3 aq. 28 w%) were all purchased from FUJIFILM Wako Pure Chemical Corporation, Ltd., Japan. All of the chemicals were used as received without further purification. Deionized water was used for all of the experiments.

4.2. Fabrication of a Cu_2O-Film-Based Bending Sensor. A Cu_2O film was fabricated on PET substrates (30 mm × 40 mm × 0.125 mm) via the spin−spray method, as

https://doi.org/10.1021/acsomega.1c04279
ACS Omega 2021, 6, 32647−32654

shown in Figure 1a. Before fabrication, the substrate was ultrasonically cleaned in deionized water for 10 min, followed by a plasma treatment (Plasma system, Diener electric, Germany, Femto) for 10 min to increase the surface hydrophilicity. The reaction and source solutions were prepared by dissolving the precursor materials in 0.7 L of deionized water. The source solution was prepared using the mixed $CuSO_4{\cdot}5H_2O$ (0.04 M) and $C_6H_8O_6$ (0.04 M) solution. $C_6H_8O_6$ was introduced as a reducing agent. Its reduction reaction in the source solution is shown in eq 3.

$$Cu^{2+} + C_6H_8C_6 \rightarrow 2Cu^{+} + C_6H_6C_6 + 2H^{+} \quad (3)$$

The reaction solution was prepared by dissolving NaOH (0.4 M) in aq. NH_3 solution (1.2 M). The reaction and source solutions were pumped to their respective nozzles at a flow rate of 0.05 L/min and sprayed onto the substrate on the rotating table (150 rpm) with a N_2 carrier gas. The rotating table was heated for the film fabrication and was maintained at a constant temperature of 70 °C during the 10 min deposition. The fabricated sample was cleaned for 10 min in water using an ultrasonic cleaner (Ultrasonic cleaner, HONDA ELECTRONICS Co. LTD., Japan, WT-200-M). The Ag paste was printed on top of the film sample at the two counter ends using the squeegee method as the contact electrodes (30 mm × 10 mm), to which Cu wires were attached, as shown in Figure 1b.

4.3. Characterization and Performance. The crystallinity and microstructure of the samples were analyzed using X-ray diffraction (XRD; BRUKER Co., USA, D8 FOCUS/TXS) at a scan angle (2θ) in a range of 20−80°. X-rays at a wavelength of 0.15418 nm were generated using a Cu−K_α source at 35 kV and 50 mA. The surface morphologies of the samples were examined using field-emission scanning electron microscopy (FESEM, HITACHI, Japan, S-4700) in a secondary electron mode at a working voltage of 8 kV. After drying the samples at 60 °C for 24 h, X-ray photoelectron spectroscopy (XPS; Physical Electronics, Inc., USA, PHI 5000) was used to investigate the chemical states. All of the XPS spectra were fitted using a numerical simulation program (XPSPEAK 41) with a Shirley background and a Lorentzian/Gaussian line shape. The presence of impurities in the samples was confirmed using attenuated total reflection Fourier transform infrared (ATR-FTIR) spectroscopy (FT-IR IRPrestige-21, Shimadzu Corp., Japan). The bending deformation of the sensor was performed by changing the distance between both of its ends, as shown in Figure 1c. The bending characteristic was evaluated using the curvature measured from the shape profile of the sensor captured by a charge-coupled device (CCD) camera. The electrical signals of the bending deformation were recorded at the same time using a Keithley 2400 digital meter at a constant voltage of 5 V. The mechanical fatigue of the sensor was investigated using bending−release cycles (Tension-Free U-shape Folding Test Jig DLDM111LH and Desktop model bending endurance tester TCDM111LH, Yuasa System Co., Ltd., Japan).

AUTHOR INFORMATION

Corresponding Author

Nobuhiro Matsushita − *Department of Materials Science and Engineering, School of Materials and Chemical Technology, Tokyo Institute of Technology, Meguro, Tokyo 152-8550, Japan*; orcid.org/0000-0001-7712-4560; Email: matsushita.n.ab@m.titech.ac.jp

Authors

Ryosuke Nitta − *Department of Materials Science and Engineering, School of Materials and Chemical Technology, Tokyo Institute of Technology, Meguro, Tokyo 152-8550, Japan*; orcid.org/0000-0003-2893-9565

Ryo Taguchi − *Laboratory for Chemistry and Life Science, Institute of Innovative Research, Tokyo Institute of Technology, Midori, Yokohama 226-8503, Japan*

Yuta Kubota − *Department of Materials Science and Engineering, School of Materials and Chemical Technology, Tokyo Institute of Technology, Meguro, Tokyo 152-8550, Japan*; orcid.org/0000-0003-2641-9136

Tetsuo Kishi − *Department of Materials Science and Engineering, School of Materials and Chemical Technology, Tokyo Institute of Technology, Meguro, Tokyo 152-8550, Japan*

Atsushi Shishido − *Laboratory for Chemistry and Life Science, Institute of Innovative Research, Tokyo Institute of Technology, Midori, Yokohama 226-8503, Japan*

Complete contact information is available at: https://pubs.acs.org/10.1021/acsomega.1c04279

Notes

The authors declare no competing financial interest.

ACKNOWLEDGMENTS

Part of this work was financially supported by the project of Creation of Life Innovation Materials for Interdisciplinary and International Researcher Development, MSL, IIR, Tokyo Institute of Technology. The authors thank Tiffany Jain, from Edanz Group (https://jp.edanz.com/ac) for editing a draft of this manuscript.

REFERENCES

(1) Wei, Y.; Chen, S.; Li, F.; Lin, Y.; Zhang, Y.; Liu, L. Highly Stable and Sensitive Paper-Based Bending Sensor Using Silver Nanowires/Layered Double Hydroxides Hybrids. *ACS Appl. Mater. Interfaces* **2015**, *7*, 14182−14191.

(2) Kim, S.; Amjadi, M.; Lee, T. I.; Jeong, Y.; Kwon, D.; Kim, M. S.; Kim, K.; Kim, T. S.; Oh, Y. S.; Park, I. Wearable, Ultrawide-Range, and Bending-Insensitive Pressure Sensor Based on Carbon Nanotube Network-Coated Porous Elastomer Sponges for Human Interface and Healthcare Devices. *ACS Appl. Mater. Interfaces* **2019**, *11*, 23639−23648.

(3) Gerboni, G.; Diodato, A.; Ciuti, G.; Cianchetti, M.; Menciassi, A. Feedback Control of Soft Robot Actuators via Commercial Flex Bend Sensors. IEEE/ASME Trans. *Mechatronics* **2017**, *22*, 1881−1888.

(4) Joo, Y.; Yoon, J.; Ha, J.; Kim, T.; Lee, S.; Lee, B.; Pang, C.; Hong, Y. Highly Sensitive and Bendable Capacitive Pressure Sensor and Its Application to 1 V Operation Pressure-Sensitive Transistor. *Adv. Electron. Mater.* **2017**, *3*, 1−10.

(5) Park, K., Il; Son, J. H.; Hwang, G. T.; Jeong, C. K.; Ryu, J.; Koo, M.; Choi, I.; Lee, S. H.; Byun, M.; Wang, Z. L.; Lee, K. J. Highly-Efficient, Flexible Piezoelectric PZT Thin Film Nanogenerator on Plastic Substrates. *Adv. Mater.* **2014**, *26*, 2514−2520.

(6) Talukdar, A.; Qazi, M.; Koley, G. High Frequency Dynamic Bending Response of Piezoresistive GaN Microcantilevers. *Appl. Phys. Lett.* **2012**, *101*, 1−6.

(7) Talukdar, A.; Qazi, M.; Koley, G. High Frequency Dynamic Bending Response of Piezoresistive GaN Microcantilevers. *Appl. Phys. Lett.* **2012**, *101*, 1−6.

(8) Luo, N.; Huang, Y.; Liu, J.; Chen, S. C.; Wong, C. P.; Zhao, N. Hollow-Structured Graphene−Silicone-Composite-Based Piezoresistive Sensors: Decoupled Property Tuning and Bending Reliability. *Adv. Mater.* **2017**, *29*, 1−9.

https://doi.org/10.1021/acsomega.1c04279
ACS Omega 2021, 6, 32647−32654

(9) Wang, Q.; Jian, M.; Wang, C.; Zhang, Y. Carbonized Silk Nanofiber Membrane for Transparent and Sensitive Electronic Skin. *Adv. Funct. Mater.* **2017**, *27*, 1−9.
(10) Sun, B.; Long, Y. Z.; Liu, S. L.; Huang, Y. Y.; Ma, J.; Zhang, H. Di.; Shen, G.; Xu, S. Fabrication of Curled Conducting Polymer Microfibrous Arrays via a Novel Electrospinning Method for Stretchable Strain Sensors. *Nanoscale* **2013**, *5*, 7041−7045.
(11) Samoei, V. K.; Jayatissa, A. H. Aluminum Doped Zinc Oxide (AZO)-Based Pressure Sensor. *Sens. Actuators, A* **2020**, *303*, No. 111816.
(12) Dong, C.; Fu, Y.; Zang, W.; He, H.; Xing, L.; Xue, X. Self-Powering/Self-Cleaning Electronic-Skin Basing on PVDF/TiO_2 Nanofibers for Actively Detecting Body Motion and Degrading Organic Pollutants. *Appl. Surf. Sci.* **2017**, *416*, 424−431.
(13) Deng, W.; Yang, T.; Jin, L.; Yan, C.; Huang, H.; Chu, X.; Wang, Z.; Xiong, D.; Tian, G.; Gao, Y.; Zhang, H.; Yang, W. Cowpea-Structured PVDF/ZnO Nanofibers Based Flexible Self-Powered Piezoelectric Bending Motion Sensor towards Remote Control of Gestures. *Nano Energy* **2019**, *55*, 516−525.
(14) Sun, S.; Zhang, X.; Yang, Q.; Liang, S.; Zhang, X.; Yang, Z. Cuprous Oxide (Cu_2O) Crystals with Tailored Architectures: A Comprehensive Review on Synthesis, Fundamental Properties, Functional Modifications and Applications. *Prog. Mater. Sci.* **2018**, *96*, 111−173.
(15) Zhao, Q.; Wang, K.; Wang, J.; Guo, Y.; Yoshida, A.; Abudula, A.; Guan, G. Cu_2O Nanoparticle Hyper-Cross-Linked Polymer Composites for the Visible-Light Photocatalytic Degradation of Methyl Orange. *ACS Appl. Nano Mater.* **2019**, *2*, 2706−2712.
(16) Deng, S.; Tjoa, V.; Fan, H. M.; Tan, H. R.; Sayle, D. C.; Olivo, M.; Mhaisalkar, S.; Wei, J.; Sow, C. H. Reduced Graphene Oxide Conjugated Cu_2O Nanowire Mesocrystals for High-Performance NO_2 Gas Sensor. *J. Am. Chem. Soc.* **2012**, *134*, 4905−4917.
(17) Zhu, H.; Wang, J.; Xu, G. Fast Synthesis of Cu_2O Hollow Microspheres and Their Application in DNA Biosensor of Hepatitis B Virus. *Cryst. Growth Des.* **2009**, *9*, 633−638.
(18) Palakollu, V. N.; Karpoormath, R.; Wang, L.; Tang, J. N.; Liu, C. A Versatile and Ultrasensitive Electrochemical Sensing Platform for Detection of Chlorpromazine Based on Nitrogen-Doped Carbon Dots/Cuprous Oxide Composite. *Nanomaterials* **2020**, *10*, 1−15.
(19) Minami, T.; Nishi, Y.; Miyata, T.; Nomoto, J. I. High-Efficiency Oxide Solar Cells with ZnO/Cu_2O Heterojunction Fabricated on Thermally Oxidized Cu_2O Sheets. *Appl. Phys. Express* **2011**, *4*, 2−5.
(20) Lai, G.; Wu, Y.; Lin, L.; Qu, Y.; Lai, F. Low Resistivity of N-Doped Cu_2O Thin Films Deposited by Rf-Magnetron Sputtering. *Appl. Surf. Sci.* **2013**, *285*, 755−758.
(21) Lai, G.; Wu, Y.; Lin, L.; Qu, Y.; Lai, F. Low resistivity of N-doped Cu_2O thin films deposited by rf-magnetron sputtering. *Appl. Surf. Sci.* **2013**, *285*, 755−758.
(22) Jeong, S. H.; Aydil, E. S. Heteroepitaxial Growth of Cu_2O Thin Film on ZnO by Metal Organic Chemical Vapor Deposition. *J. Cryst. Growth* **2009**, *311*, 4188−4192.
(23) Xu, H. Y.; Chen, C.; Xu, L.; Dong, J. K. Direct Growth and Shape Control of Cu_2O Film via One-Step Chemical Bath Deposition. *Thin Solid Films* **2013**, *527*, 76−80.
(24) Lim, Y. F.; Chua, C. S.; Lee, C. J. J.; Chi, D. Sol-Gel Deposited Cu_2O and CuO Thin Films for Photocatalytic Water Splitting. *Phys. Chem. Chem. Phys.* **2014**, *16*, 25928−25934.
(25) Shinagawa, T.; Ida, Y.; Mizuno, K.; Watase, S.; Watanabe, M.; Inaba, M.; Tasaka, A.; Izaki, M. Controllable Growth Orientation of Ag_2O and Cu_2O Films by Electrocrystallization from Aqueous Solutions. *Cryst. Growth Des.* **2013**, *13*, 52−58.
(26) Nitta, R.; Kubota, Y.; Kishi, T.; Yano, T.; Matsushita, N. One-Step Direct Fabrication of Phase-Pure Cu_2O Films via the Spin-Spray Technique Using a Mixed Alkaline Solution. *Mater. Chem. Phys.* **2020**, 243.
(27) Shimada, Y.; Matsushita, N.; Abe, M.; Kondo, K.; Chiba, T.; Yoshida, S. Study on Initial Permeability of Ni-Zn Ferrite Films Prepared by the Spin Spray Method. *J. Magn. Magn. Mater.* **2004**, *278*, 256−262.
(28) Wagata, H.; Ohashi, N.; Taniguchi, T.; Katsumata, K. I.; Okada, K.; Matsushita, N. Control of the Microstructure and Crystalline Orientation of ZnO Films on a Seed-Free Glass Substrate by Using a Spin-Spray Method. *Cryst. Growth Des.* **2010**, *10*, 4968−4975.
(29) Lin, H. E.; Katayanagi, Y.; Kishi, T.; Yano, T.; Matsushita, N. A Solution-Processed Tin Dioxide Film Applicable as a Transparent and Flexible Humidity Sensor. *RSC Adv.* **2018**, *8*, 30310−30319.
(30) Vesel, A.; Junkar, I.; Cvelbar, U.; Kovac, J.; Mozetic, M. Surface Modification of Polyester by Oxygen- And Nitrogen-Plasma Treatment. *Surf. Interface Anal.* **2008**, *40*, 1444−1453.
(31) Zhu, C.; Osherov, A.; Panzer, M. J. Surface Chemistry of Electrodeposited Cu_2O Films Studied by XPS. *Electrochim. Acta* **2013**, *111*, 771−778.
(32) Swarnkar, R. K.; Singh, S. C.; Gopal, R. Effect of Aging on Copper Nanoparticles Synthesized by Pulsed Laser Ablation in Water: Structural and Optical Characterizations. *Bull. Mater. Sci.* **2011**, *34*, 1363−1369.
(33) Chen, J. Y.; Zhou, P. J.; Li, J. L.; Li, S. Q. Depositing Cu2O of Different Morphology on Chitosan Nanoparticles by an Electrochemical Method. *Carbohydr. Polym.* **2007**, *67*, 623−629.
(34) Dourado, A. H. B.; da Silva, A. G. M.; Pastrián, F. A. C.; Munhos, R. L.; de Lima Batista, A. P.; de Oliveira-Filho, A. G. S.; Quiroz, J.; de Oliveira, D. C.; Camargo, P. H. C.; Córdoba de Torresi, S. I. In Situ FTIR Insights into the Electrooxidation Mechanism of Glucose as a Function of the Surface Facets of Cu_2O-Based Electrocatalytic Sensors. *J. Catal.* **2019**, *375*, 95−103.
(35) Kuwahara, K.; Taguchi, R.; Kishino, M.; Akamatsu, N.; Tokumitsu, K.; Shishido, A. Experimental and Theoretical Analyses of Curvature and Surface Strain in Bent Polymer Films. *Appl. Phys. Express* **2020**, *13*, No. 056502.
(36) Taguchi, R.; Akamatsu, N.; Kuwahara, K.; Tokumitsu, K.; Kobayashi, Y.; Kishino, M.; Yaegashi, K.; Takeya, J.; Shishido, A. Nanoscale Analysis of Surface Bending Strain in Film Substrates for Preventing Fracture in Flexible Electronic Devices. *Adv. Mater. Interfaces* **2021**, *8*, No. 2001662.
(37) Sun, Y.; Thompson, S. E.; Nishida, T. Physics of Strain Effects in Semiconductors and Metal-Oxide-Semiconductor Field-Effect Transistors. *J. Appl. Phys.* **2007**, *101*, No. 104503.
(38) Fiorillo, A. S.; Critello, C. D.; Pullano, A. S. Theory, Technology and Applications of Piezoresistive Sensors: A Review. *Sens. Actuators, A* **2018**, 156−175.
(39) Kleimann, P.; Semmache, B.; Le Berre, M.; Barbier, D. Stress-Dependent Hole Effective Masses and Piezoresistive Properties of-Type Monocrystalline and Polycrystalline Silicon. *Phys. Rev. B: Condens. Matter Mater. Phys.* **1998**, *57*, 8966−8971.
(40) Taguchi, R.; Kuwahara, K.; Akamatsu, N.; Shishido, A. Quantitative Analysis of Bending Hysteresis by Real-Time Monitoring of Curvature in Flexible Polymeric Films. *Soft Matter* **2021**, *17*, 4040−4046.

https://doi.org/10.1021/acsomega.1c04279
ACS Omega 2021, 6, 32647−32654